Depth-shifting of shallow water guide source observations

Lisa M. Zurk and , , Brian H. Tracey and , and

Citation: The Journal of the Acoustical Society of America **118**, 2224 (2005); doi: 10.1121/1.2010309
View online: http://dx.doi.org/10.1121/1.2010309
View Table of Contents: http://asa.scitation.org/toc/jas/118/4
Published by the Acoustical Society of America

Depth-shifting of shallow water guide source observations

Lisa M. Zurk[a)]
Electrical and Computer Engineering, Portland State University, 1900 SW Fourth Avenue, FAB 160-17, Portland, Oregon 97207

Brian H. Tracey[b)]
NEUROMetrix, Inc., 62 Fourth Ave., Waltham, Massachusetts 02451

(Received 17 November 2004; revised 21 June 2005; accepted 4 July 2005)

In theory, matched field processing offers the significant benefit of higher signal gains and increased localization capability. However, this has not been robustly observed in practice because of inherent uncertainties about details of the shallow water propagation environments which limit the prediction of the channel response. The use of guide sources to directly measure the transfer function between source and receiver arrays has been proposed as a means for reducing mismatch. However, the guide source measurement only provides a measured transfer function at the guide source location. In this paper a method of depth-shifting guide source observations is proposed, making it possible to estimate transfer functions for points in the ocean other than the guide source location. The proposed depth-shifting process does not require knowledge of environmental parameters. The theoretical background for the technique is developed below and its range of applicability is examined © *2005 Acoustical Society of America.* [DOI: 10.1121/1.2010309]

PACS number(s): 43.30.Wi, 43.30.Bp [EJS] Pages: 2224–2233

I. INTRODUCTION

Passive sonar performance in shallow water can be degraded because these environments support complex multipath propagation and often include multiple loud surface interferers. Matched field processing (MFP), which incorporates a propagation model to determine the replicas used in beamforming, has been proposed as a way to recover the losses incurred due to multipath propagation and provide increased source localization.[1] Adaptive processing, in particular adaptive MFP (AMFP) can provide the ability to null surface interference. Receive arrays with significant vertical aperture can support discrimination between surface and submerged sources and, if accurate environmental inputs are available, can achieve significant adaptive rejection of surface sources. Under ideal situations, AMFP can provide improved performance in both localization and detection of sources.

In practice the performance gains possible from AMFP are difficult to achieve. High ambiguities typically exist in the MFP output, especially for arrays with limited vertical aperture, which limits interferer rejection. The motion of the targets and interferers can be a significant problem, introducing additional signal loss, smearing source peaks, and consuming adaptive degrees of freedom.[2] However, for arrays with significant vertical aperture the most important limitation on MFP performance is that precise information on the underwater channel is generally not available. The mismatch between the computed and actual array steering vectors can result in loss of array gain and, for adaptive processing, signficant target self-nulling.

A number of approaches have been proposed to deal with the problem of environmental mismatch in MFP. Algorithms can be designed that attempt to reduce sensitivity by directly building a model of the environmental uncertainty into the processing.[3–5] Alternatively, geoacoustic inversion methods can be used to estimate more accurate seabed parameters, which are typically the source of greatest environmental uncertainty. Inversions can be done using either transmissions of known wave forms from calibrated sources[6,7] or from sources of opportunity such as loud merchant ships.[7]

Other authors have suggested the use of *guide sources* for mitigating environmental uncertainty.[8,9] Guide sources may be calibrated sources deployed for an experiment or can be sources of opportunity such as surface ships, whose position might be obtained from an offboard sensor. In either case the guide source can be used to determine the acoustic response across the array, eliminating the need to predict the response using a propagation model. This response is immediately known for the source-receiver path of the guide source, but it is still unknown for sources at alternate locations.

The approach presented here attempts to determine the response of a source by translating the observed response from the guide source. In previous work,[10] translation of a response from one source range to another was demonstrated by utilizing multifrequency data. However, the guide source will generally be located at a different depth than the target of interest, meaning that a method of translating in *depth* is desired. This is particularly true when the guide source is a surface ship and the target of interest is a submerged source. In this paper a method of "depth shifting" the guide source response using a vertical line array (VLA) is presented. With knowledge of the guide source location, this vector can then be shifted in depth to provide a steering vector for beamforming to alternate depths. Thus, a replica vector is obtained

[a)]Electronic mail: zurkl@cecs.pdx.edu
[b)]Work was done when the author was with MIT Lincoln Laboratory, 244 Wood Street, Lexington, Massachusetts 02420.

without the need for environmental knowledge or the use of a propagation model.

The work presented here is similar in some respects to work done by Conti *et al.* for a time-reversal mirror application.[11] Conti *et al.* used image processing techniques to extract the curvature of the field received from an impulsive source across a fully spanning VLA. This curvature was related to an image source contribution. By adjusting the curvature before playing back the time-reversed signal, the location of the time-reversal focal point was shifted in depth and range. The approach in the following accomplishes a similar shifting but applies to cw sources, rather than the short-duration wave forms used in time-reversal operations.

The first section to follow outlines the theoretical background for depth shifting. The depth-shifted observation (or replica vector) is formed by applying an operator to the actual guide source observation. The choice of this operator is motived by the derivation of an approximate mode orthogonality condition. A calculation for estimating the location of the depth-shifted peak is shown and conditions for the depth-shifting operation to be accurate are discussed. Finally, simulation results are used to demonstrate the technique. The use of an alternate depth-shifting operation is also explored.

II. THEORETICAL BACKGROUND FOR DEPTH SHIFTING

The normal mode representation of the field at frequency ω and time t that is present on a sensor at depth z due to a unit normalized source at a range r_s and depth z_s can be written as

$$p(z_s,z,r_s;\omega,t)=\frac{i\rho(z_s)}{(8\pi)^{1/2}}\sum_{m=1}^{M}\Psi_m(z_s)\Psi_m(z)\frac{e^{i[k_m(\omega)-\alpha_m(\omega)]r_s(t)}}{\sqrt{k_m(\omega)r_s(t)}}, \tag{1}$$

where Ψ_m is the mode function, k_m is the horizontal wave number, α_m is the attenuation constant of the mth mode, and M is the total number of propagating modes. For simplicity, the explicit reference to frequency ω in Eq. (1) will be omitted in subsequent equations except when the frequency dependence is not clear.

One useful characteristic of the mode functions is their orthonormalacy relationship, which can be written as

$$\int_0^D \Psi_l(z)\Psi_m(z)=\delta(l-m), \tag{2}$$

where the integration is computed over the water column of depth D. In MFP, the above-noted relationship can be used to simplify the inner product of pressure fields sampled along a fully spanning VLA to a weighted summation over a single mode.[10] In this section, a similar relationship is pursued, but one that involves not only the mode functions but their spatial derivatives. The rationale is that there is a correspondence between mode number m and source depth, so that shifting in mode number produces an analogous effect to shifting in depth. This central idea will be motivated by the derivation in this section, followed by the expressions for the MFP output produced in the following section.

The derivation begins by noting that the depth dependence in Eq. (1) is contained entirely in the mode functions Ψ_m, which are a function of two parameters: the vertical mode wave number $k_{z,m}$ and source depth. An assumption is made that this dependence is on the *product of the two*, i.e., $\Psi_m(z)$ can be considered as a function of the form $f(k_{z,m}z)$. This is consistent with the Wentzel–Kramers–Brillion (WKB) approximation for mode shapes and eigenvalues.

Under this assumption, the partial derivatives with respect to depth and wave number, respectively, can be written as

$$\frac{\partial}{\partial z}\Psi_m(z)=g(k_{z,m}z)\left[k_{z,m}+\frac{\partial k_{z,m}}{\partial z}z\right]\cong g(k_{z,m}z)k_{z,m},$$
$$\frac{\partial}{\partial k_{z,m}}\Psi_m(z)=g(k_{z,m}z)z, \tag{3}$$

where the unknown function $g(k_{z,m}z)$ has been introduced as a common product of the two differentiations [for example, if $\Psi_m(z)=\sin k_{z,m}z$, then $g=\cos k_{z,m}z$]. In calculating the depth derivative, the depth dependence of the vertical wave number has been neglected. The unknown function g can be eliminated to give

$$\frac{\partial}{\partial k_{z,m}}\Psi_m(z)=\frac{\partial}{\partial z}\Psi_m(z)\frac{z}{k_{z,m}}, \tag{4}$$

which can be approximated using a centered finite difference:

$$\frac{\partial}{\partial k_{z,m}}\Psi_m(z)\approx\frac{\Psi_{m+1}(z)-\Psi_{m-1}(z)}{k_{z,m+1}-k_{z,m-1}}. \tag{5}$$

The results so far have introduced a parametrization of the mode functions and have shown how its derivatives are related. A new approximate orthogonality expression for the mode functions is now derived.

The standard mode orthogonality condition in Eq. (2) can be used to write the following difference expression:

$$\int_0^D[\Psi_{l+1}(z)-\Psi_{l-1}(z)]\Psi_m(z)dz=\delta(l+1-m)-\delta(l-1-m). \tag{6}$$

(This is obtained by applying the orthogonality condition twice, then subtracting the two results.) The resulting expression includes a term similar to the centered difference in Eq. (5), thus inserting and simplifying gives

$$\int_0^D z\frac{\partial}{\partial z}\Psi_l(z)\frac{k_{z,l+1}-k_{z,l-1}}{k_{z,l}}\Psi_m(z)dz=\delta(l+1-m)-\delta(l-1-m). \tag{7}$$

Now, the horizontal wave numbers are assumed to have a linear dependence on mode number:

$$k_{z,l}=q(z)l. \tag{8}$$

In general q will be a function of depth, but as noted earlier, this difference has been assumed to be weak. The difference between vertical wave numbers in Eq. (7) can then be sim-

plified, giving a new (but approximate) orthogonality expression for the mode functions:

$$\int_0^D z\frac{\partial}{\partial z}\Psi_l(z)\Psi_m(z)dz \approx \frac{l}{2}[\delta(l+1-m)-\delta(l-1-m)]. \tag{9}$$

The right-hand side above will be nonzero when either delta function is satisfied, i.e., when $m=l\pm1$. Thus the approximate orthogonality condition will hold between nearest-neighbor modes. The expression is approximate because of the first-order finite difference used to represent the vertical wave number derivative. If desired, higher-order approximations to the finite difference could be used to capture additional off-diagonal mode cross-talk terms.

From numerical experiments, it was observed that a similar approximate orthogonality can be obtained if the depth-shifted replica is taken to be simply the depth-derivative of the guide source data [without the factor of z on the left-hand side (LHS) of Eq. (9)]. This behavior can be explained in terms of the mode shapes expected for modes that are well above cutoff. In this case the mode shapes tend towards $\sqrt{(2/D)}\sin k_{z,l}z$, with vertical wave numbers given by $k_{z,l}=\pi l/D$. The integral of mode m with the depth derivative of mode l can be calculated to be

$$\int_0^D \frac{\partial}{\partial z}\Psi_l(z)\Psi_m(z)dz = \frac{l}{D}\left(\frac{1-\cos\pi(m-l)}{m-l}+\frac{1-\cos\pi(m+l)}{m+l}\right), \tag{10}$$

which will be identically zero for $l=m\pm2k$, where $k=[0,2,4,\ldots]$. The resulting zeros help to reduce cross-talk and sidelobe levels. Note that the factor of $1/D$ above results in lower cross-correlation values than were seen in Eq. (9). The different scaling between the two depth-shifting operations is removed when the depth-shifted replica is normalized.

III. MODIFIED BARTLETT PROCESSOR

The output from a Bartlett matched field processor evaluated at a position of (z,r) can be written as

$$P(z,r)=|\bar{w}^H(z,r)\cdot\bar{y}|^2, \tag{11}$$

where $\bar{w}(z,r)$ is the $Nx1$ weight vector and $\bar{y}$ is the received response across the N-element array. Since the intent of this paper is to describe an algorithm for the structured shifting of MFP output peaks, the case considered here is that of a single deterministic source (or target) at position (z_s,r_s), so that $\bar{y}=\bar{y}(z_s,r_s)$ and $P(z_s,r_s)$ is the matched field output at the target range and depth. [In general, for a signal in presence of noise, the beamformer output is a stochastic quantity that should be evaluated with an expectation operator. However, the goal of the present work is not to evaluate the signal to noise performance, but instead the ability to shift the beamformer focus direction by varying the steering vector applied to a deterministic signal. Thus, for the theoretical development we consider the case of deterministic MFP with the understanding that the usual signal and noise models apply (see, for example, Ref. 1). In the numerical simulations, background white noise at 60 dB is included.] For the standard Bartlett processor, $\bar{w}=\bar{w}_{\text{model}}$ and the weight is the normalized output of a propagation model (commonly referred to as the "replica" vector). Accurate detection and localization is heavily dependent on accurate knowledge of the ocean environment, which is typically not available in practice.

In this paper, a modified Bartlett processor is presented where the weight vectors are obtained not from model output, but from manipulation of a guide source response. Thus, the "matching" occurs between previously observed fields, and there is no loss due to model parameter mismatch. This modified Bartlett processor has the form given in Eq. (11) but with $\bar{w}=\bar{w}_{\text{guide}}$ computed from a guide source, and the exact form will now be presented. The weight vectors are obtained from observing the acoustic field from a guide source (the guide source SNR is assumed to be high enough so the effects of noise are negligible).

In the previous section, an approximate mode orthogonality relationship was presented which resulted from computing the derivative of the mode functions with respect to depth. To utilize this relationship in a modified Bartlett processor, the depth-shifted "replica" vectors are computed from

$$\bar{v}^H(z,r)=\boldsymbol{z}\odot\frac{\partial}{\partial z}\bar{x}(z_g,r_g), \tag{12}$$

where $\bar{x}(z_g,r_g)$ is the field received from the guide source, $\bar{z}$ is a vector of depths at each phone location, and $\odot$ indicates the Hadamard product, or element-wise multiplication. The depth-shifted weight is then calculated as

$$\bar{w}(z_s,r_s)=\frac{\bar{v}(z_s,r_s)}{|\bar{v}(z_s,r_s)|}. \tag{13}$$

The use of this weight vector can be evaluated by substituting Eqs. (12) and (13) into Eq. (11) to give

$$P(z,r)=|\bar{w}^H(z,r)\cdot\bar{y}(z,r)|^2=C\left|\boldsymbol{z}\odot\frac{\partial}{\partial z}\bar{x}(z_g,r_g)\cdot\bar{y}(z,r)\right|^2, \tag{14}$$

where C is a normalization constant. With sufficiently fine spacing, the depth derivative can be approximated by a finite difference equation, with the elements of the shifted replica given by

$$v_k(z_s,r_s)=z_k\frac{x_{k+1}(z_g,r_g)-x_{k-1}(z_g,r_g)}{2\Delta z}, \tag{15}$$

where k is the index to a particular hydrophone in the array and Δz is the depth spacing between hydrophones. [Effects of the discretization introduced in Eq. (15) will be discussed and examined in the numerical simulations.] Assuming that the acoustic field from the guide source and the target can be expressed in normal modes as given in Eq. (1) then gives

$$P(z,r) = C\left|\sum_{n}^{N} z_{rn}\frac{\partial}{\partial z}x_n(z_g,r_g)y_n(z_s,r_s)\right|^2 = C'\left|\sum_{l}^{L}\sum_{m}^{M}\left(\sum_{n}^{N} z_{rn}\frac{\partial}{\partial z}\Psi_l(z_g,r_g)\Psi_m(z_s,r_s)e^{i(k_l r_g - k_m r_s)}\right)\right|^2, \tag{16}$$

where the spatial summation in the inside brackets is evaluated at the $n=1,\ldots,N$ elements of the array, z_{rn} is the depth of the nth hydrophone, and C' is a new constant that contains the additional terms in Eq. (1). It can be seen that in Eq. (16) the summation is the discrete approximation of the LHS of Eq. (9); substituting in the delta function on the right-hand side of the equality then gives

$$P(z,r) = \left|\sum_{m}^{M}(m-1)\Psi_m(z)\Psi_{m-1}(z_g)e^{i(k_m r - k_{m-1}r_g)} - (m+1)\Psi_m(z)\Psi_{m+1}(z_g)e^{i(k_m r - k_{m+1}r_g)}\right|^2, \tag{17}$$

which is the modified Bartlett output evaluated at source position z, r and using the guide source response for depth shifting. This differs from the conventional MFP expression because the quantity is evaluated at mode indexes m and $m\pm1$ (the conventional expression contains only the index m for a fully spanning VLA). Thus, the maximum output does not occur when $z_g=z_s$ and $r_g=r_s$, but for some other "shifted" location.

In the simulation and analytic results to follow, the problem is restricted to that of obtaining depth-shifted replicas at the guide source range. Thus $r=r_s=r_g$ in Eq. (17). In this case the output power of the processor becomes

$$P(z,r) = \left|\sum_{m}^{M}(m-1)\Psi_m(z)\Psi_{m-1}(z_g)e^{i(k_m - k_{m-1})r} - (m+1)\Psi_m(z)\Psi_{m+1}(z_g)e^{i(k_m - k_{m+1})r}\right|^2. \tag{18}$$

Depth-shifted replicas at different ranges will be discussed in Sec. III B.

A. Location of shifted peak

Expressions for the location of the shifted peak can be derived using a WKB approach to describe the vertical wave numbers and mode shapes. The depth shifted peak will be calculated assuming that $r=r_s=r_g$, as described in Eq. (18). The power output will be maximized when terms match on a mode-by-mode basis. The shifted peak z_s should satisfy the following:

$$\Psi_m(z_s) = \Psi_{m-1}(z_g)e^{i(k_m - k_{m-1})r}, \qquad \Psi_m(z_s) = \Psi_{m+1}(z_g)e^{i(k_m - k_{m+1})r}. \tag{19}$$

An estimate of the shifted location is found using the following steps:

(1) the WKB approximation is used to express modes as a sum of up- and down-going waves.
(2) Equation (19) is rewritten as four equations, satisfying the up- and down-going portions of the wave field.
(3) Approximate values for the shifted location are found.

The steps involved are shown in the Appendix. As a final result, the shifted depth is given as

$$z_s \simeq z_g \pm \frac{q}{k_m}r. \tag{20}$$

Thus the depth-shifting process will cause two shifted peaks in depth to appear for every possible guide source depth. The Appendix shows that this is because the up- and down-going portions of the wave field are shifted differently. To first order, the mode wave numbers will be comparable to the medium wave number, so an approximate estimate for depth-shifting is given by

$$z_s \simeq z_g \pm \frac{q}{k_0}r. \tag{21}$$

As noted earlier, for modes well above their cut-off frequency, $q=\pi/D$. Using this value together with the frequency, guide source range, and guide source depth, the locations of the depth-shifted peaks can be estimated. Note that the depth shift is frequency-dependent, so that if multiple frequencies are available (i.e., the sources have some bandwidth or multiple tonals) these can be used to generate shifts at multiple target depths. Thus, Eq. (21) provides a means for generating a family of target depth values. Finally, it will be shown in Sec. III B, processing using the ambiguity introduced by the $\pm$ in Eq. (21) can be resolved by application of the invariance principle.

The analytic results can also be used to qualitatively explain several features that will be seen in simulation results. First, Eq. (20) shows that the exact location of the shifted peak is mode-dependent. Thus if the modes have very different phase speeds, a smearing of the peak location will result. Second, the derivations above assume that the variation in vertical wave number with depth can be neglected. To the extent that this is not true, i.e., significant sound speed gradients exist, an additional defocusing of the depth-shifted peak may be expected.

B. Range invariance shifting

The expression in Eq. (21) gives the relationship between the guide position z_g, r_g and a single target depth of z_s with $r_s=r_g=r$ at the single frequency ω. If the guide source is a broadband source, the concept of using the invariance principle to shift in range[10,12] can be utilized. As will be shown in this section, this provides the ability to consider $r_s \neq r_g$ and utilize multiple observations from the guide source when it moves in range.

The objective is to acquire a weight vector which allows one to beamform to a source at position z_s, r_s and at a target frequency of ω. Assume that observations have been acquired for a guide source traveling in range and radiating over some (broad) acoustic bandwidth. Then, consider the

Bartlett output using one of these weight vectors acquired when the guide source is at $z=z_g$, $r=r_g$ and the guide response at the frequency $\omega_g=\omega+\Delta\omega$ is used to give

$$P(z_s,r_s)=\left|\sum_m^M (m-1)\Psi_m(z)\Psi_{m-1}(z_g)e^{i(k_m(\omega)r_s-k_{m-1}(\omega+\Delta\omega)r_g)} - (m+1)\Psi_m(z)\Psi_{m+1}(z_g)e^{i(k_m(\omega)r_s-k_{m+1}(\omega+\Delta\omega)r_g)}\right|^2, \tag{22}$$

where the frequency dependence has been explicitly introduced for clarity and the assumption has been made the Ψ does not vary considerably between ω and $\omega+\Delta\omega$. (The frequency increment $\Delta\omega$ is considered small enough so that $\Delta\omega/\omega<0.1$.) To continue, follow the approach described in the Appendix of utilizing the WKB approximation and equating arguments of the exponentials to obtain the following expression for the processor peak:

$$z_s=\frac{1}{qm}[z_g q(m-1)+(k_m(\omega)(r_s)-k_{m-1}(\omega+\Delta\omega)r_s+\Delta r)], \tag{23}$$

where the substitution of $r_s=r_g+\Delta r$ has been used. Approximate the wave number k_m as

$$k_m(\omega+\Delta\omega)=\sqrt{(k_0+\Delta k)^2-q^2m^2}\approx k_0\left(1-\frac{q^2m^2}{2k_0^2}-\frac{\Delta k}{k_0}\right) \tag{24}$$

to give (see the Appendix for details)

$$k_m(\omega+\Delta\omega)-k_{m-1}(\omega)\approx -q^2\frac{m}{k_0}-\Delta k. \tag{25}$$

Retaining dominant terms then gives the following depth shift operation:

$$z_s\simeq z_g\pm\left[\frac{q}{k_0}r_g-\frac{1}{qm}(\Delta k r_g-k_0\Delta r_g)\right]. \tag{26}$$

The last term of Eq. (26) goes to zero when it satisfies the invariance relationship given by Brehovskih[12] as (for $\beta=1$)

$$\frac{\Delta\omega}{\omega}=\frac{\Delta r}{r}. \tag{27}$$

When Eq. (27) is satisfied, Eq. (26) reduces to the form of Eq. (21) except that the Bartlett processor peaks for guide range $r_g\neq r_s$, and each value of r_g provides a different depth shift as per Eq. (26). When responses from a number of guide positions are observed [e.g., the guide moves in range, r_g) this implies choosing the frequency $\omega=\omega_g-\Delta\omega$ to satisfy Eq. (27), resulting in the ability to shift to z_s as given in (26)]. For a guide source that has sufficient frequency extent, this fact can be used to resolve the ambiguity introduced by the ± in Eq. (21).

IV. DEPTH-SHIFTING ALGORITHM

To summarize the preceeding sections, the algorithm for depth shifting using a guide source is described in the following list.

(1) The acoustic pressure $\bar{x}(z_g,r_g)$ across the array due to a high SNR guide source is observed and retained, with the guide position (i.e., $z=z_g$ and $r=r_g$) known from other information. This acquisition potentially occurs for a number of guide source ranges as the guide transverses the region and over a substantial bandwidth.
(2) For each discrete frequency band and source range, the derivative of the pressure with respect to depth is computed. For a vertical array with sufficient depth sampling, this may be approximated by using a finite difference approximation as was utilized in the derivation in the previous section. Alternately, an acoustic vector sensor could be used to measure the particle velocity, from which the derivative of the pressure may be calculated.
(3) The resulting derivatives are then normalized to unit norm and stored as array weight vectors. Each weight vector is associated with an unique target range and depth (r_s,z_s) through the relationships given in Eqs. (21) and (26). Note that with sufficient range observations and signal bandwidth weight vectors can be obtained for all possible target locations.
(4) The output of the Bartlett processor in Eq. (11) is computed by applying the weight vectors from the previous step to pressure across the array to determine power in the direction of interest $(r=r_s,z=z_s)$. Note that if multiple steering vectors are available for a single source depth (due to multiple guide source ranges and broad signal bandwidth) these can be used to resolve the ambiguity arising from the ± sign in Eqs. (21) and (26).

The above-noted procedure is particularly interesting when a surface ship is considered as a potential guide source. In this case the algorithm is readily applied (with $z_g\equiv 2$ m) as surface interference typically has a high SNR and its position may be obtained from a surface radar or shipping lane information. Furthermore, the source is typically broadband and can be observed at multiple ranges as the ship moves—a fact which was exploited in Sec. III B.

V. SIMULATION RESULTS

Simulation results were generated using an environmental model based parameters gathered during the Santa Barbara Channel experiment (SBCX). Numerical results are shown for 148 and 235 Hz, which were tones used during the experiment, but no actual data results from SBCX are presented here. This is due to the fact that a data-driven evaluation of the depth shifting algorithm requires the presence (and position knowledge) of a guide source at multiple ranges, along with observations of a target source. It is hoped that constructing data collection opportunities for such an evaluation may occur in the future, but in absense of this data, the current work presents the theoretical background and only simulated results.

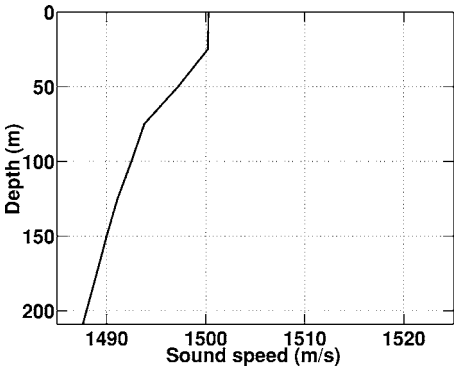

FIG. 1. Sound speed profile (SSP) for Santa Barbara Channel environment.

For all simulation results, a range-independent normal mode simulation based on KRAKEN output was used.[13] Figure 1 shows the sound speed profile used for the simulations, and Table I lists the assumed geoacoustic properties of the SBCX site. For comparison, results will also be shown for a 209-m-deep Pekeris waveguide with a constant sound speed of 1500 m/s in the water column overlying an acoustic half-space (parameters c_c=1800 m/s, ρ=2 g/cm^3, and α_c =0.04 dB/λ).

A. Mode orthogonality results

This section examines the approximate mode orthogonality condition derived in previous sections. Mode correlation matrices are calculated for a verticle line array (VLA) that fully spans the water column with 1 m vertical separation between phones. The array gives excellent sampling so the underlying orthogonality of the mode shapes is seen. While not plotted, evaluation of the "standard" mode orthogonality condition [i.e., Eq. (2)] gives cross-talk between modes (or off-diagonal elements of a mode correlation matrix) at very low values (less than −15 dB).

Figure 2 graphically shows the approximate orthogonality condition predicted by Eq. (9). For convenience, the figure is produced by weighting the right-hand side of Eq. (9) with a factor of $2/l$, so that perfect orthogonality would result in nonzero (first) off-diagonal terms with the value one, and zeros elsewhere. The depth-shifting operation $\boldsymbol{z}\odot\partial/\partial z$ is calculated using a centered finite difference on the mode shapes. As predicted, because of the depth-shifting operation, the correlation is highest between each mode and its two nearest neighbors but there is nonzero cross-talk between modes. This is believed to be a result of the approximations utilized in the derivation of the new mode orthogonality condition (such as the linear dependence of the vertical wave number on mode index) which are less applicable at the higher order modes that undergo increased bottom interaction, as discussed in the next section. This increased cross-talk may be expected to lead to higher sidelobe levels on the depth-shifted ambiguity surface.

TABLE I. Parameters for geoacoustic model used in SBCX data: z =depth from surface; c_c=compressional sound speed; ρ=density; α_c =compressional wave attenuation.

z(m)	c_c(m/s)	ρ(g/cm^3)	α_c(dB/λ)
209	1607	1.95	0.37
309	1702	1.95	0.37
309	1862	1.98	0.035
609	2374	1.98	0.035
609	2374	2.03	0.04

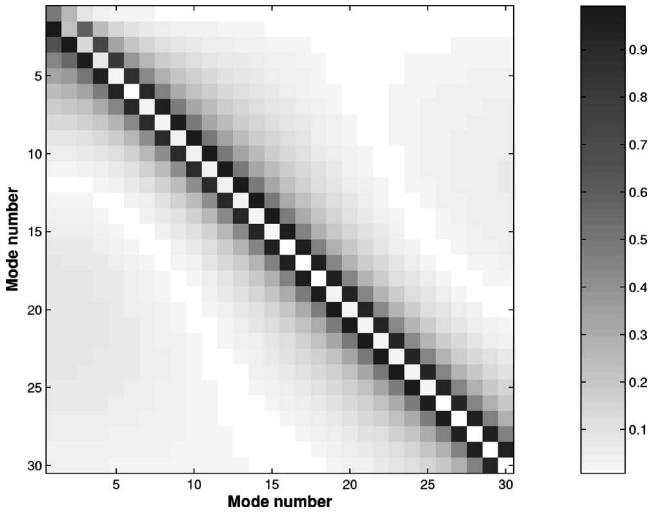

FIG. 2. Mode correlation matrix (outer product) between depth-shifted and original modes for fully spanning VLA in SBCX environment. Output is produced as specified in the left-hand side of Eq. (9) and the figure is plotted with a multiplicative factor of $1/2$ so that perfect agreement would result in a value of one on the off-diagonals, and zero elsewhere. Frequency is 235 Hz.

The accuracy of the discrete evaluation of both the standard orthogonality and the approximate differential orthogonality relationship depends on the spacing and extent of the discrete integral in Eqs. (2) and (9), respectively. Deviations from orthonormality occur for arrays that either do not span the entire water column or have insufficient array spacing. In Fig. 3, the mode correlation matrices for both orthogonality relations are shown for an array that is undersampled [Figs. 3(a) and 3(b)] or only partially spans the water column [Figs. 3(c) and 3(d)]. It can be seen from the figure that the accuracy of the discrete approximation deteriorates for both orthogonality relationships, and would result in decreased performance for a VLA without sufficient sampling.

This observed degradation is perhaps more pronounced for the new orthogonality relationship, and is particularly more noticeable at the higher mode numbers. It is believed that this is because those modes experience greater attenuation and loss due to bottom interaction. In the theoretical derivation, it was assumed that the vertical wave numbers increase approximately linearly with mode number, and will clearly not be the case for the higher modes. However, with sufficient energy at the lower modes (which is frequently the case for long range propagation scenarios) the losses due to deviations of the higher order modes may be negligible. Note also that other common sources of array degradation (such as error in element position) will apply to the mode correlation and hence also to the depth shifting.

Because the SBCX environment has a downward refracting sound speed profile (SSP), it does not exactly satisfy the assumptions made in deriving Eq. (9). As a check, depth-

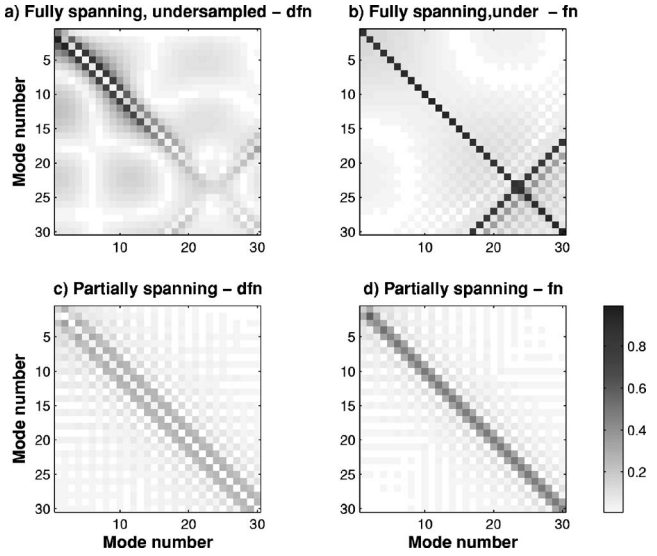

FIG. 3. Mode correlation matrix for SBCX environment using Eq. (9) (left-hand column) and Eq. (2) (right-hand column), plotted with a multiplicative factor of 1/2. Simulated VLA has inadequate spacing ($1.5*\lambda=9$ m) in (a) and (b), or covers the top half of the water column in (c) and (d). For both standard and new orthogonality relationships, degradation occurs as the array becomes less capable. Frequency is 235 Hz.

shifted correlation matrices for a variety of ocean environments were calculated. The mode correlation matrix for the cases considered were nearly identical to that calculated for the SBCX environment, indicating the specific ocean parameters do not have a critical effect on the results.

As discussed earlier, an alternate depth-shifting operation can be carried out by applying only the depth derivative to the guide source observation. The behavior of this alternate depth-shifted replica is seen from the mode correlation matrix in Fig. 4. This figure again shows high correlation between nearest-neighbor modes, but a "checkerboard" pattern is seen in the output. This pattern was predicted from

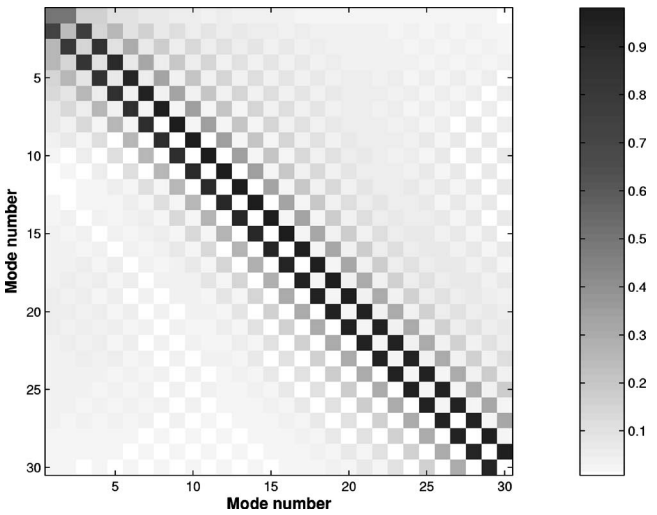

FIG. 4. Mode correlation matrix between depth-shifted and original modes for fully spanning VLA in SBCX environment, using the simple depth-derivative operation. The "checkerboard" pattern predicted by Eq. (10) is seen, giving reduced mode cross-talk as compared to Fig. 2.

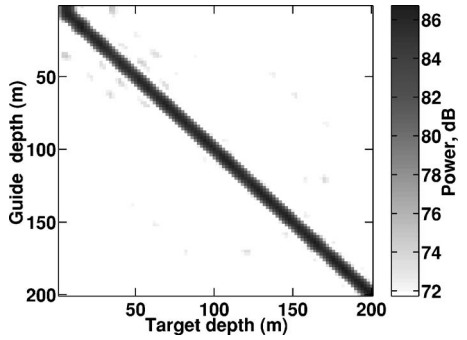

FIG. 5. Bartlett output for 2.5 km guide source at $f=235$ Hz in SBCX environment with no depth shifting.

Eq. (10). The different scalings between the two depth-shifting operations are removed when the depth-shifted replica is normalized.

B. Depth-shifted results

In this section the depth-shifting operation is applied to simulated guide source measurements to verify that shifting occurs and to understand how performance depends on the environment. The receive array used for simulation has a similar geometry to the VLAs used in SBCX, consisting of a bottom-mounted VLA with 30 hydrophones spaced at 5 m separation in the vertical, spanning roughly 80% of the water column. The uppermost phone in the array is at a depth of 5 m.

For reference, a simulation was run showing MFP output at 235 Hz using a guide source without applying the depth shifting algorithm developed in this paper. The result, shown in Fig. 5, is for the case $r_g=r_s=2.5$ km. The output is plotted as a function of the guide source depth and the target depth, z_g and z_s, respectively. As expected, the unshifted guide source can only be used to produce output at the depth of the guide source.

Figures 6 and 7 show the result of applying the depth-shifting algorithm to data collected from guide sources at ranges of 2.5 and 4 km, respectively, at a frequency of 235 Hz. The depth-shifted output is again produced at the same range as the guide source ($r_g=r_s$). In Fig. 8, the depth-shifted result is produced at $f=148$ Hz, with all other parameters remaining the same. In all three figures, as predicted by

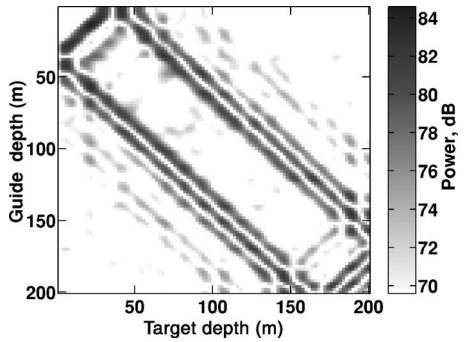

FIG. 6. Depth shifted output as given in Eq. (18) for 2.5 km guide source radiating at $f=235$ Hz in SBCX environment. Note that the peak is split in two as predicted, with predicted peaks at $z_s=z_g\pm40$ m.

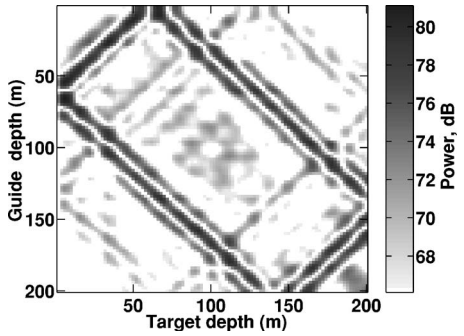

FIG. 7. Depth shifted output as given in Eq. (18) for 4.0 km guide source radiating at $f=235$ Hz in SBCX environment. Note that the peak is split in two as predicted, with predicted peaks at $z_s=z_g\pm64$ m.

theory, shifted peaks appear at two depths for every guide source depth. It can be seen from examination of the figures that diversity in source range and/or frequency produces multiple target depths or shift values (i.e., the ability to locate sources at multiple possible depths z_s).

Evaluating Eq. (21) with the values for the ocean depth, guide source range, and frequency used in the simulation example gives an estimate of the predicted shifted depths. For the $f=235$ Hz case, at 2.5 km in range a peak in output is expected for $z_s=z_g\pm40$ m, while for the 4 km range peaks are predicted at $z_s=z_g\pm64$ m. For $f=148$ Hz at 4 km range the peak is predicted at $z_s=z_g\pm101$ m. All these values are in good agreement with the simulation results, even though the environment is not an isospeed channel. This suggests that the relationship between the guide depth and the shifted depth may be only weakly sensitive to details of the environment.

As noted earlier good results can be obtained by using a simple depth derivative applied to the guide source data. Figure 9 and 10 shows the depth-shifted outputs for 2.5 and 4 km sources, respectively. The sidelobe levels obtained using this depth-shifting operation are lower than those seen in Figs. 6 and 7, due to the reduced cross-talk between modes seen in Fig. 4.

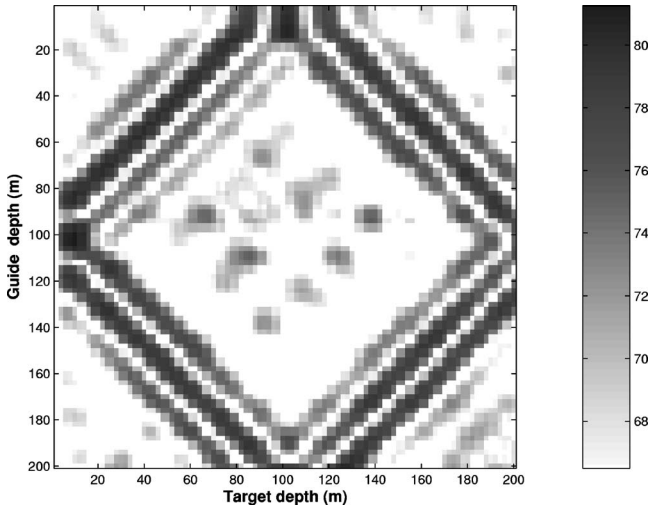

FIG. 8. Depth shifted output as given in Eq. (18) for 4.0 km guide source radiating at $f=148$ Hz in SBCX environment. Note that the peak is split in two as predicted, with predicted peaks at $z_s=z_g\pm101$ m.

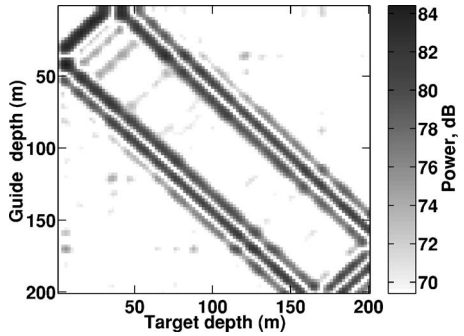

FIG. 9. Depth shifted output for 2.5 km guide source radiating at $f=235$ Hz, SBCX environment, obtained by applying a depth-derivative to the guide source data. Note that sidelobes are suppressed compared to Fig. 6.

The above-noted derivations assume that the vertical wave number for each mode is only weakly dependent on depth. When sound speed varies with depth, this is no longer strictly true and some defocusing can be expected. Additional simulations were run to better understand the sensitivity to sound speed profile. The simpler depth-derivative depth-shifting operation was used for these simulations. First, results were generated for a Pekeris waveguide, which has constant sound speed in the water column. Results were then generated for an environment with the extremely steep downward refracting sound speed profile shown in Fig. 11, having the same bottom properties as the SBCX site. Results for the Pekeris environment are shown in Fig. 12, while results for the steep SSP environment are seen in Fig. 13 (guide source range is 2.5 km in both cases). For the Pekeris waveguide, little evidence of mismatch loss and defocusing is seen. Increased mismatch is seen for the steep SSP environment. These results support the idea that the depth-shifted replicas will be most accurate when the change between the sound speed at the guide source depth and at the shifted peak depths are relatively small.

Comparing Figs. 9 and 12 to the standard MFP result (Fig. 5) shows a loss of signal energy in the depth-shifted results. This loss is believed to result from the increased weighting that depth-shifting places on high-order modes (shown in Fig. 2), which distorts the replicas. This signal loss will increase the SNR requirements for successful source lo-

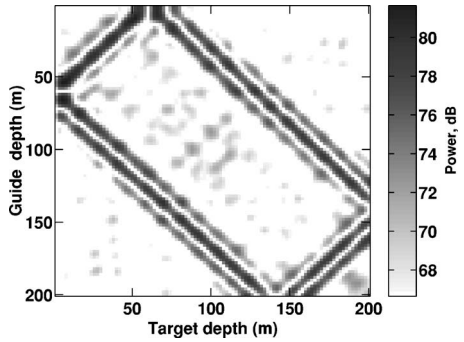

FIG. 10. Depth shifted output for 4 km guide source radiating at $f=235$ Hz, SBCX environment, obtained by applying a depth-derivative to the guide source data. Note that sidelobes are suppressed compared to Fig. 7.

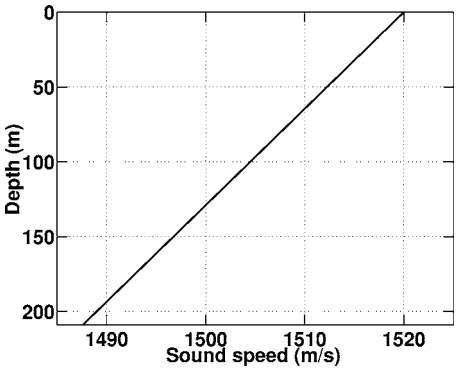

FIG. 11. Steep downward refracting sound speed profile designed to stress depth-shifting technique.

calization using depth-shifting. However, mismatch losses are also present in standard MFP due to environmental uncertainty. For the SBCX experiment, where good environmental calibration was available, mismatch losses for MFP were typically 1–2 dB.[2] For environments where ocean parameters are poorly known, the mismatch introduced by depth-shifting may be less than for standard MFP.

C. Invariance depth-shifted results

The theory of Sec. III B suggests that a response shifted in both range and depth can be produced by utilizing a guide with a broadband response as per Eq. (26). The results shown in Fig. 14 were produced by using the response from a guide source at range $r_g = r_s - \Delta r$ and frequency $\omega_g = \omega_s + \Delta\omega$ for a target range of 4 km and frequency at $f_s = 2\pi\omega_s = 148$ Hz. As previously seen in Fig. 8, the guide response produces a depth-shifted focus at $z_s = z_g \pm 101$ m when $\Delta r = 0$ (i.e., $r_g = r_s$) and $\Delta f = \Delta\omega/(2\pi) = 0$. When the modified Bartlett output in Eq. (18) is calculated using the guide response at $\Delta f = 10$ Hz, the peak occurs at the target depth z_s as given in Eq. (26) but for the guide range satisfying the invariance relationship in Eq. (27) : $\Delta r = \Delta f / f \times r_s$. In Fig. 14 the MFP output is plotted as a function of guide range and target depth with a peak occuring at 4.0 km range for $\Delta f = 0$ (left-hand plot) and at 4.3 km in range for $\Delta f = 0$ (right-hand plot); both of which which agree with the predicted values.

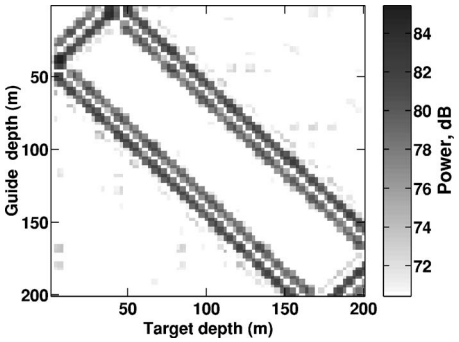

FIG. 12. Depth shifted output for 2.5 km guide source radiating at $f = 235$ Hz, Pekeris waveguide environment. Depth-shifting is done by applying a depth-derivative to the guide source data. Note that output is slightly cleaner than for the SBCX case.

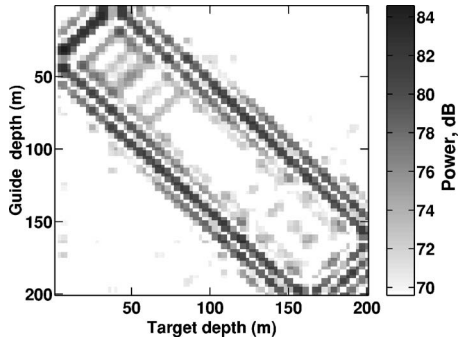

FIG. 13. Depth shifted output for 2.5 km guide source radiating at $f = 235$ Hz, for environment with steep sound speed profile. Depth-shifting is done by applying a depth-derivative to the guide source data. Note the increased sidelobe levels as compared to the environments which have smaller sound speed gradients.

VI. CONCLUSIONS

While matched field processing holds the promise of increased target gain and localization accuracy, MFP performance can be seriously degraded by uncertainties of the underwater environment. Guide sources at known positions in the ocean may be used to address this problem by directly measuring the source-to-receiver transfer functions for use in processing. In this work, a new algorithm for extending guide source observations for use in MFP has been introduced. This algorithm provides a method of observing the response (e.g., steering vector) from a guide source at one depth, and translating it to another depth. It relies on a new approximate orthogonality relationship which shifts the modes that contribute to the MFP output. The technique does not require environmental inputs, though performance will degrade for environments with steep sound speed profiles. The depth shifting operators examined here, which use a depth derivative to form the shifted replicas, introduce some signal losses that will increase SNR requirements for successful source localization. The development of other depth-shifting operations that aim to minimize this loss may be an interesting topic for further investigation.

ACKNOWLEDGMENTS

The authors would also like to thank William Kuperman, Hee Chun Song, and Philippe Roux for helpful feedback about depth-shifting concepts.

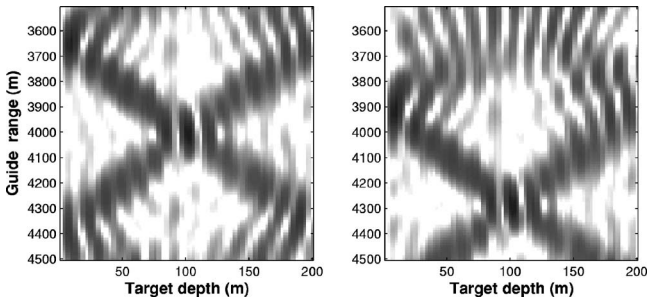

FIG. 14. Depth shifted MFP output for 4.0 km target at 235 Hz plotted as a function of target depth and guide range. The guide source is at 2 m depth and the response is at 148 Hz (left-hand plot) and 158 Hz (right-hand plot). The shifting of $\Delta f = 10$ Hz produces a shift in the range peak from 4.0 km to 4.3 km. Location of the target depth is given by Eq. (26).

APPENDIX: WKB CALCULATION FOR SHIFTED PEAK LOCATION

As in Eq. (8), the vertical wave numbers are assumed to be linearly related to mode number. The mode functions are approximated using the WKB approach, which models the mode as a sum of up- and down-going plane waves with angles that may vary in depth:

$$\psi_l(z) = Be^{i\int_0^z q(z)ldz} + Ce^{-i\int_0^z q(z)ldz}. \tag{A1}$$

The relative amplitudes B and C of the up- and down-going waves depend on boundary conditions of the problem.

The WKB approximation can be expected to be accurate for modes that are well above their cutoff frequencies. Another simplified ocean environment that yields modes which fit the above-mentioned model is the so-called ideal waveguide, which consists of an isospeed ocean with a pressure release surface and bottom. In this case the vertical wave number is given by $k_{z,l}=(\pi/D)l$, where D is the ocean depth, and mode shapes are given by $\sqrt{(2\rho/D)}\sin k_{z,l}z$. The ideal waveguide model can be a good approximation for modes that are well above their cut-off frequencies.

Using the WKB approximation for the mode shape, the two equations in Eq. (19) are split into four, by requiring the up-going and down-going parts of the modes to satisfy the equations separately. The first equation is

$$B_m e^{i\int_0^{z_s} qmdz} = B_{m-1} e^{i\int_0^{z_g} q(m-1)dz} e^{i(k_m - k_{m-1})r}, \tag{A2}$$

where the depth dependence of $q(z)$ is not shown explicitly.

A first step in completing this calculation is to find the horizontal wave number difference between adjacent modes. Given the above-mentioned assumptions, the horizontal wave number is given by

$$k_m = \sqrt{k_0^2 - q^2 m^2}, \tag{A3}$$

where k_0 is the medium wave number (ω/c). It is fairly easy to show that

$$k_{m-1} = k_m \sqrt{1 + \frac{q^2(2m-1)}{k_m^2}}. \tag{A4}$$

Approximating the square root operator and making the assumption that modes higher than the first few are important (so that $2m \gg 1$), an approximate horizontal wave number difference is found as

$$k_m - k_{m-1} \approxeq -q^2 \frac{m}{k_m}. \tag{A5}$$

Two simplifying assumptions are now made. First, the mode amplitude terms B_m and B_{m-1} are assumed to be are roughly equal and are divided out of Eq. (A2). The equality will then be satisfied if the arguments to the exponential terms are equal. Next the assumption is made, as above, that the vertical wave number term q is approximately constant with depth. In that case the depth integrals become trivial, and the depth of the shifted peak is given by

$$\begin{aligned} z_s &= \frac{m-1}{m} z_g - \frac{q}{k_m} r_s, \\ z_s &\approxeq z_g - \frac{q}{k_m} r_s, \end{aligned} \tag{A6}$$

where the approximation made on the second line will be valid beyond the first few modes. Carrying out a similar calculation with the down-going wave gives a second solution:

$$z_s \simeq z_g + \frac{q}{k_m} r_s. \tag{A7}$$

The same two solutions are found by equating the up- and down-going waves in the second line of Eq. (19). These results can be used to estimate the shifted locations of the depth peaks.

[1] A. Baggeroer, W. Kuperman, and P. Mikhalevsky, "An overview of matched field methods of ocean acoustics," IEEE J. Ocean. Eng. **18**, 401–424 (1993).

[2] L. Zurk, N. Lee, and J. Ward, "Source motion mitigation for adaptive matched field processing," J. Acoust. Soc. Am. **113**, 2719–2731 (2003).

[3] J. Krolik, "Matched-field minimum variance beamforming in a random ocean channel," J. Acoust. Soc. Am. **92**, 1408–1419 (1992).

[4] A. Richardson and L. Nolte, "*A posteriori* probability source localization in an uncertain sound speed, deep ocean environment," J. Acoust. Soc. Am. **89**, 2280–2284 (1991).

[5] P. Daly, "Stochastic matched field processing for localization and nulling of acoustic sources," Ph.D thesis, Massachusetts Institute of Technology, 2000.

[6] M. Siderius, M. Snellen, D. Simons, and R. Onken, "An environmental assessment in the Strait of Sicily: Measurement and analysis techniques for determining bottom and oceanographic properties," IEEE J. Ocean. Eng. **18**, 401–424 (1993).

[7] D. Knobles, R. Koch, L. Thompson, K. Focke, and P. Eisman, "Broadband sound propagation in shallow water and geoacoustic inversion," J. Acoust. Soc. Am. **113**, 205–222 (2003).

[8] M. Siderius, D. Jackson, D. Rouseff, and R. Porter, "Multipath compensation in shallow water environments using a virtual receiver," J. Acoust. Soc. Am. **102**, 3439–3449 (1997).

[9] L. Fialkowski, M. Collins, W. Kuperman, J. Perkins, L. Kelly, A. Larsson, J. Fawcett, and L. Hall, "Matched-field processing using measured replica fields," J. Acoust. Soc. Am. **107**, 739–746 (2000).

[10] A. Thode, "Source ranging with minimal environmental information using a virtual receiver and waveguide invariant theory," J. Acoust. Soc. Am. **108**, 1582–1594 (2000).

[11] S. Conti, P. Roux, and M. Fink, "Depth and range shifting of a focal spot using a time-reversal mirror in an acoustic waveguide," Appl. Phys. Lett. **80**, 3647–3649 (2002).

[12] L. M. Brekhovskiih and Y. Lysanov, *Fundamentals of Ocean Acoustics*, 2nd ed. (Springer, Berlin, 1991).

[13] M. Porter, "The KRAKEN normal mode program," SACLANT Undersea Research Centre Technical Report SM-245, 1991.